 doi:10.20944/preprints201810.0177.v1

Surface modification of the bulk metallic glass $Zr_{46}Cu_{36.8}Ag_{9.2}Al_8$ triggered by millisecond laser irradiation

Alexandra A. Shlykova, Mikhail F. Gasanov

Department of Physics, Derzhavin Tambov State University, 392000 Tambov, Russia

Alexandr Nasedkin

Division of Biological Physics, Department of Physics, Chalmers University of Technology, SE-412 96 Gothenburg, Sweden

Viktor A. Fedorov

Department of Physics, Derzhavin Tambov State University, 392000 Tambov, Russia

Abstract

Zirconium based bulk metallic glasses are industrially valuable materials which commercial market grows rapidly. Surface modification of these metallic glasses by high-intensity lasers is relatively new and costly treatment promising great advantages over classical surface processing methods. In this work we perform the case study of surface modification of $Zr_{46}Cu_{36.8}Ag_{9.2}Al_8$ metallic glass by high-intensity millisecond laser beam. Our results suggest chemical deposition of atmospheric oxygen and nitrogen in the laser-melted surface area and its surroundings. Zirconium nitride layer was detected in the middle of laser-irradiated area. Nanocrystals embedded in the amorphous matrix were also formed on the surface. Overall, our findings suggest possibilities for improvement of mechanical characteristics of the studied metallic glass.

Keywords: Zirconium, bulk metallic glass, laser material processing, amorphous, nanocrystals, surface modification, glass transition

1. Introduction

Bulk metallic glasses (BMG) are relatively novel sort of materials attracting much of the attention because of their unique combination of mechanical properties. High strength and high elasticity of BMGs in combination with their corrosion resistance made those materials a prospective candidates for industrial applications [1, 2, 3, 4, 5]. Yet, the wide use of BMGs is heavily limited by their low glass transition temperatures. Much of the technological processing takes place at temperatures exceeding the glass transition temperature of the

Preprints (www.preprints.org) | NOT PEER-REVIEWED | Posted: 9 October 2018 doi:10.20944/preprints201810.0177.v1

BMGs: heating will inevitably result in partial crystallization and phase separation and following structural relaxation ultimately worsens crucial mechanical properties [6, 7, 8, 9, 10]. Future estimates place a large accent on combining several techniques for processing of BMGs [11].

Prospectively, laser material processing represent an alternative to the traditional welding [12]. Laser pulses could selectively influence surface of the material, whereas controllable duration of the pulse opens wide perspectives for adjustable damage in the irradiated area [13]. Thus, laser manipulations of amorphous alloys attract interest as industrial processing method. Such, powder coating by amorphous layers [14, 15], laser beam welding [6, 8], laser surface hardening by the knock waves [16, 17], laser microscopic treatment of the surface [18] and laser technologies for the preparation of the micro- and nano- structures were developed [19].

Particular focus in laser processing is given to the surface crack healing which should substantially increase the plastic flow limit. Plastic deformations in metallic glasses occurs by means of shear bands. A cluster of shear bands concentrated into a thin line leads to the intense friction heating, decrease in viscosity and following crack initiation [20]. Such clusters are normally formed about 10 nm below the surface which make them different from dislocations [21]. The primary shear band in the BMG could be stopped by e.g. the secondary bands in order to perform crack retardation [22, 23]. One of such methods is formation of crystal phases and composites on the surface. A very similar effect of crack retardation can be achieved with laser undercutting followed by release of thermo-elastic stresses.

The downside of the laser-based treatment is in induced penchant of the material toward fatigue damage [24]. Such, decrease of the micro-hardness induced by formation of the cracks in a grain-growth region is observed in the heat-affected area as a result of the laser heating [7]. On the contrary, the increase of both strength and plasticity is observed due to partial crystallization [25]. Moreover, heating leads to the surface oxidation of metallic glasses that, in turn, requires atmosphere monitoring during manufacturing process. However, the influence of the oxidation can be minimal and the sorption processes can improve the surface quality, decrease friction coefficient, increase surface micro-hardness and resistance to corrosion [26].

Millisecond-long laser pulses are among the most suitable for the laser surface processing. Lifetime of heat dissipation by the electrons is about 10^{-12}-10^{-13} s which is several orders of magnitude faster compared to the laser pulse duration. These conditions minimize ablation, and as a consequence, increase the quality of surface treatment due to the formation of more homogeneous melt layer. Thus, investigation of millisecond time-domain of laser pulses is interesting from the perspective of controllable variation of mechanical properties of BMGs [27, 28].

BMGs containing zirconium is a wide class of materials used for protective and structural elements in agressive environments [29, 30, 31, 29]. Additionally, zirconium-based materials has a number of unique properties, one of which is high biocompatibility, thus enabling their use in medical applications [32, 33,

Preprints (www.preprints.org) | NOT PEER-REVIEWED | Posted: 9 October 2018 doi:10.20944/preprints201810.0177.v1

34, 31, 35, 36].

This work has been devoted to follow surface modification of the bulk metallic glass $Zr_{46}Cu_{36.8}Ag_{9.2}Al_8$ upon millisecond laser irradiation. The process and formed structures have been characterized by combination of optical microscopy, X-ray diffraction and nanoindentation as well as computational modeling.

2. RESULTS

2.1. Nanocrystals are formed upon melting

Electron micrographs show two areas: the crater formed upon laser melting and the bare surface clearly separated by the border (Figure 1a and b). The inner area is roughly equal to the size of the laser spot. Taking into account the energy of the pulse, melting would definitely take place in this area. Surface morphology (Figure 1b) suggests that the outer ring is a flow shear area.

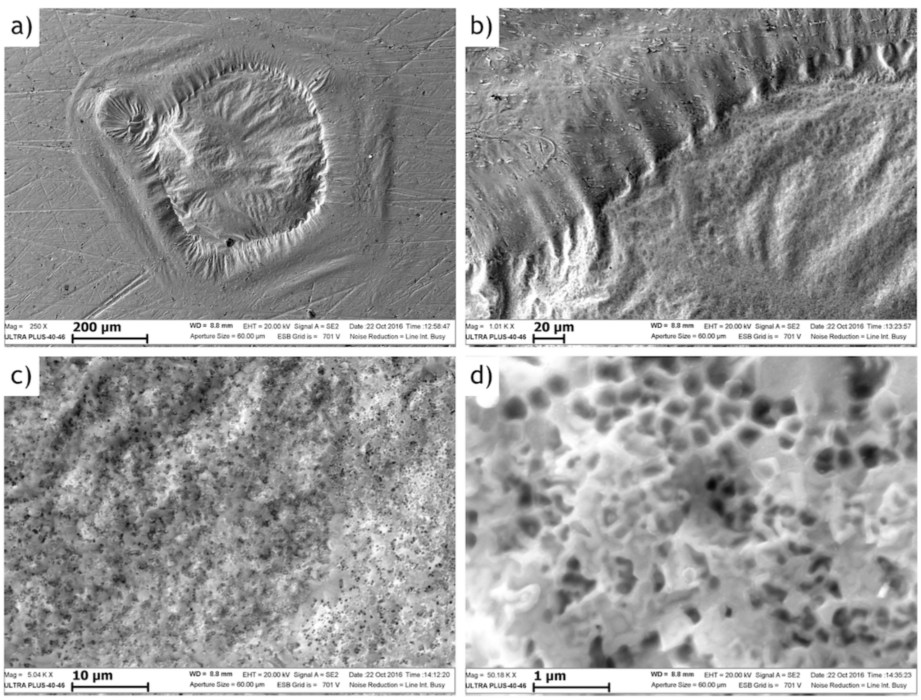

Figure 1: **Micrographs of the surface in the laser-melted area.** a) The crater, b) the area of the thermo-plastic shears magnified from figure (a). Plots c) and d) show nanocrystals from the center of the crater.

High-resolution imaging revealed nanocrystals in the center of the crater showed in Figure 1c and d. In order to further characterize the surface, we performed X-ray diffraction (XRD) measurements. The XRD spectrum showed a combination of both diffuse and crystalline forms (Figure 2) indicating that the nanocrystals are embedded in the amorphous matrix on the surface. Observed

 doi:10.20944/preprints201810.0177.v1

XRD peaks were fit with numerous diffraction patterns in order to identify chemical composition of the nanocrystals. The fitting by peak position and intensity identified Zr_2Cu, Zr_7Cu_{10}, ZrO_2 and ZrO crystallines. The latter two are typically formed during oxidation of zirconium amorphous alloys [37, 38].

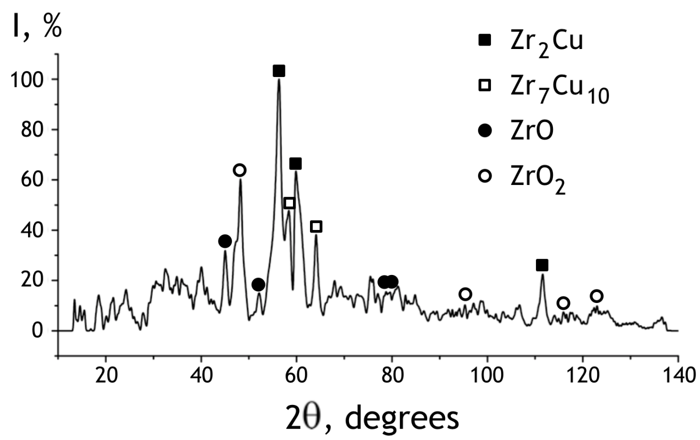

Figure 2: **X-ray diffraction pattern collected from the center of the crater.** The spectrum is a combination of diffuse and crystalline signals. Diffraction peaks for Zr_2Cu, Zr_7Cu_{10}, ZrO and ZrO_2 are assigned.

2.2. Surface composition

Chemical composition measured along the radius confirms the large quantities of surface oxygen present in the crater (Figure 3). Oxygen concentration increases to the border of the welding zone. Additionally, large quantity of the nitrogen was identified in the center of the crater. The sum of oxygen and nitrogen along the radius is approximately constant (50 %) in the crater.

2.3. Temperature and heat flow

To evaluate temperature and heat flow in the crater we have performed corresponding simulations. From simulations we determined that spontaneous temperature rise exceeds the melting temperature of the sample as far as 350 μm from the center of the laser spot. That value is larger than the value 220-240 μm that could be extracted from the raw image by assuming the shear bands form on the border of the melting zone (Figure 1a and b). The temperature profile from simulation is shown in Figure 4a. By following the isotherm on the border of the crater Figure 4a, we have identified that the melting area extend up to 60 μm below surface at the center of the crater. Surface temperature as a function of time and distance from the center of the crater is shown in Figure 4b.

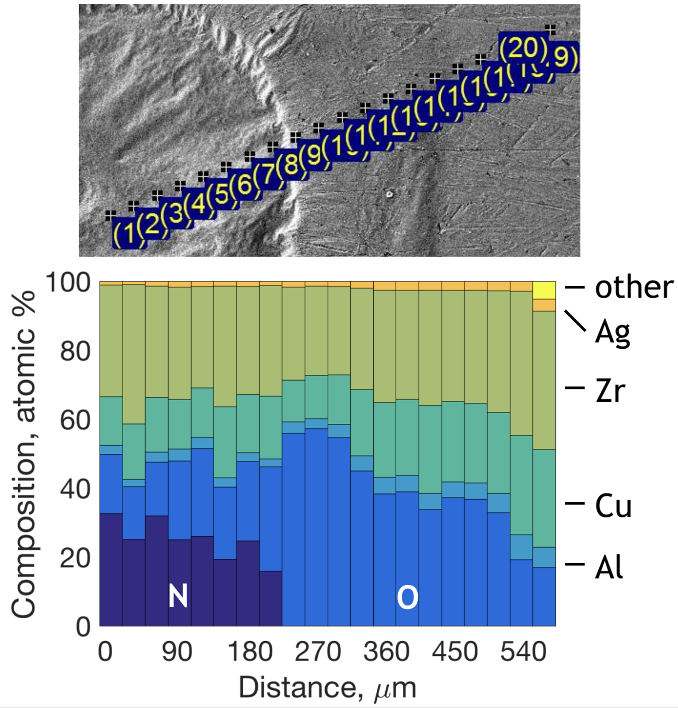

Figure 3: **Surface composition measured along the radius of the crater.** Top plot shows settings from instrument setup. Points where chemical composition was measured are located 30 μm from each other. b) Element distribution along the radius of the crater.

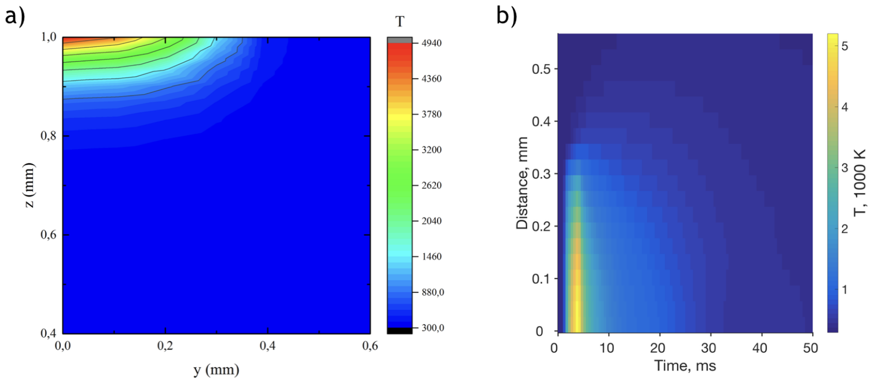

Figure 4: **Temperature distribution in the sample.** a) The snapshot of temperature distribution in the sample taken at the end of laser pulse. The top of the plot (z=1) corresponds to the surface of the sample. The radius of laser spot was 300 μm. b) Temperature profile as function of time and distance from the sample. The origin corresponds to the center of the crater and offset by $t = -1$ ms prior to the laser pulse.

3. DISCUSSION

High fractions of oxygen and nitrogen absorbed on the surface point to chemical deposition on the surface. Indeed, fraction of the oxygen absorbed into zirconium matrix at high temperatures could be significant. Due to the high surface activity [39] and high affinity of oxygen to zirconium, absorbed oxygen could consist up to 29 wt.% at 2173 K [40]. Oxygen penetrates easily into the zirconium lattice and fills the octahedral discontinuities, decreased the chemical mobility of zirconium. As a result the relative mobility of silver and aluminum increased since some zirconium is participating in chemical reactions with oxygen. Overall, the atomic mobility at crystallization is decreased and the relative impurity index increases.

Diffraction pattern shows crystalline formation of ZrO and ZrO_2 alongside with crystals detected by electron microscopy. It is anticipated that the high temperatures of the sample short after the laser pulse (Figure 4b) lead to the large absorption of molecular oxygen and following chemical reactions with metals of the sample, upon which the significant fraction of oxygen is bound to the oxides on the surface.

Additionally to the oxygen, there is significant fraction of the nitrogen detected only in the center of the crater. Similarly to the oxygen, the nitrogen is expected to be chemically bound to the modified surface of the sample. Nitrogen is less chemically active compared to the oxygen, as a consequence it would react with metals at higher temperatures compared to the latter one.

As an attempt to characterize the chemistry of occurring reactions, we calculated activation energy for oxygen and nitrogen deposition. This was based on the highest surface temperature obtained from theoretical modeling. The Arrhenius plot of concentration versus inverse temperature shows nearly linear dependence, which allows us to suggest purely activation character of occuring reactions (Figure 5). Activation energies of chemical deposition calculated from Arrhenius plots are 44 ± 14 kJ/mol for nitrogen and 2.2 ± 0.9 kJ/mol for oxygen deposition, based on 95 % confidence interval estimates.

Fraction of copper and zirconium in the sample allows to suggest that only these two metals can form significant quantities of nitrides and oxides detected on the surface. Copper nitride Cu_3N has low content of the nitrogen, thus its occurence in the center of the crater can not explain high nitrogen content. On the other hand, activation energy for nitrogen deposition correlates with previously reported value 37.4 kJ/mol for nitridation of the bulk zirconium sample [41]. Zirconium nitride can also form by oxidizing ZrO_2 films. However, high activation energy of this reaction (240 ± 10 kJ/mol [42]) prevents it from being dominant in our case.

Although the fraction of oxygen is significant on the peripheree and outside the crater, the composition of oxides in this area is unclear. Determined activation energy is too low compared to respective values for zirconium oxide (110-198 kJ/mol [43]), copper oxide (40-111 kJ/mol [44]) and aluminium oxide (156 kJ/mol [45]) formed from surface oxidation of corresponding metals. The decrease in activation energy was previously observed for copper oxide due

Preprints (www.preprints.org) | NOT PEER-REVIEWED | Posted: 9 October 2018 doi:10.20944/preprints201810.0177.v1

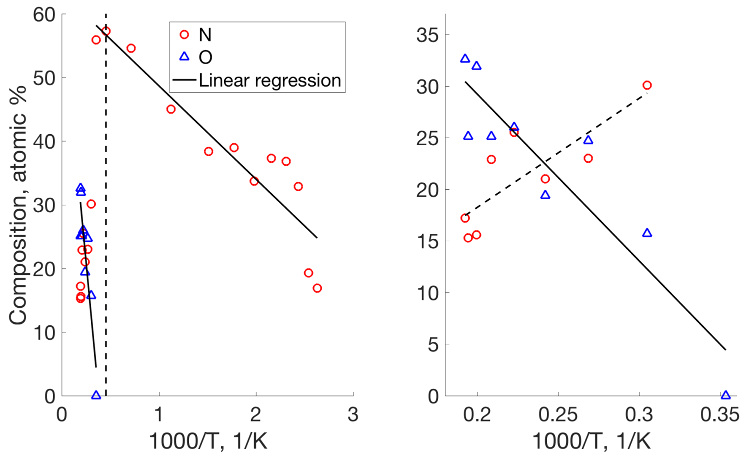

Figure 5: **Arrhenius plot of the chemical deposition.** The left hand side plot shows the whole range of distances measured experimentally. Dashed line roughly indicate the border of the crater. The right hand side plot shows magnified center of the crater. The dashed line shows linear fit of the oxygen concentration in the center of the crater.

to the formation of non-protective whisker layer [44]. Yet, the value observed in this work (2.2±0.9 kJ/mol) is at least one order of magnitude lower, thus, unravelling exact mechanism of oxidation and significant lowering of activation energy requires further investigation.

From the practical perspective, laser treatment of the surface is most interesting in preventing formation and transmission of shear bands that are the main reason for worsening mechanical characteristics of bulk metallic glasses. Formation of nanocrystals is one of the methods to prevent transmission of shear band [46, 27, 7, 47, 48, 49, 50]. Detection of the crystallines in this work is one of the aspects indicating potential for industrial applications. Additional measurement of microhardness of the sample in the laser-melt area gives a value of ≈6 GPa, which is around the hardness of the bare metallic glass. The relative inexpensiveness of the laser treatment procedure employed in this work and no special sample environment will allow us to hope that our results will particularly contribute to the wider adaptation of laser-based surface treatments.

4. Conclusion

We have investigated the surface of $Zr_{46}Cu_{36.8}Ag_{9.2}Al_8$ bulk metallic glass modified by millisecond laser pulse. The surface of the sample analysed by means of optical and electron microscopy and X-ray diffraction combined with computer modeling. We have detected the uptake of nitrogen by the surface in the center of laser-formed crater and uptake of oxygen by the large area inside and outside the crater. Activation energy for nitrogen deposition suggest the formation of the zirconium nitride in the center of the crater. Chemical origin of oxides remain unclear. Some of these crystals are most probably formations of ZrO_2 which fingerprints are probed by diffraction pattern.

Crystallization observed in the center of the crater pave ways for improvement of mechanical properties of this specific metallic glass by e.g. localization of transmitting shear bands in order to prevent premature mechanical damage. Taking into account economical aspects of milllisecond laser maintenance and cost, we believe that this study presents some interest for industrial applications.

5. Acknowledgements

We are thankful to the Swedish National Infrastructure for Computing (SNIC) for providing access to computer resources at Chalmers Centre for Computational Science and Engineering (C3SE). We are also grateful to Vitaly A. Khonic (Voronezh State Pedagogical University, Russia) for differential scanning calorimetry measurements and analysis. The work was partially supported by the Russian Foundation for Basic Research, project number RFBR 15-42-03206.

6. Materials and Methods

6.1. Sample preparation and structure control

Composite alloy $Zr_{46}Cu_{36.8}Ag_{9.2}Al_8$ (99.995 %) was produced at the Institute of Solid State Physics Russian Academy of Sciences, Chernogolovka, Moscow District. Metals were melt by induction heating, then melt jet quenched in the copper bath with constant cooling rate 200 K/s controlled by digitalized thermocouples. Temperature distribution inside the bath was homogeneous. Produced bulk metallic glass melt ($2 \times 5 \times 60$ mm^3) was quality-controlled by X-ray diffraction (wavelength 0.5668 A) at the synchrotron radiation facility at Kurchatov Institute, Moscow. The raw sample piece was further cut by diamond blade to the smaller sample pieces ($2 \times 5 \times 3$ mm^3) and further mechanically polished.

Structure of the cut sample before the laser irradiation was monitored by X-ray diffractometer *Rigaku Ultima IV CuK*α. X-ray reflectivity from the laser-affected area were performed by diffractometer *Diffrey 401 CrK*α.

6.2. Differential scanning calorimetry

The glass transition temperature (T_g) and the temperature of crystallization (T_c) were defined by differential scanning calorimetry (DSC) measurements at *Mettler-Toledo DSC1* instrument. Calorimetry scans were performed at constant heating rate of 20 K/min. Figure 6 shows DSC scans with subsequent analysis.

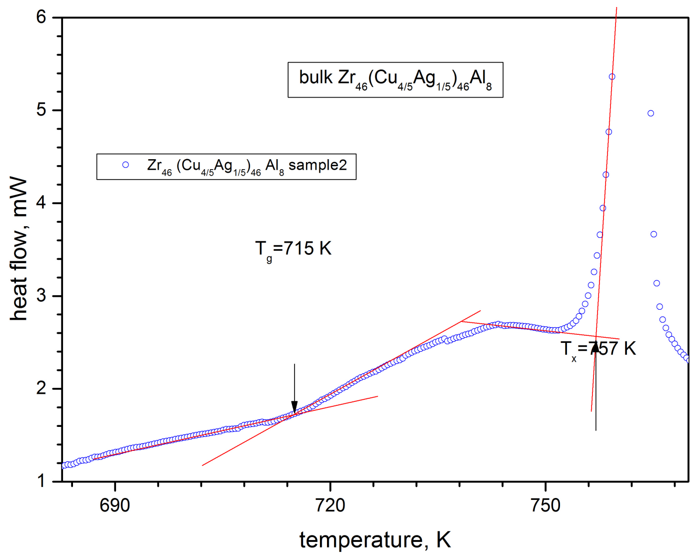

Figure 6: **DSC curve of the sample.** Different thermal transitions assigned by instrumentation software are also shown.

6.3. Laser irradiation

Surface of the sample was irradiated by single impulse of Nd:YAG laser operating at the wavelength λ=1064 nm. Duration of the pulse was 3 ms and the total energy delivered to the sample was 3$\pm$0.3 J. Radius of the laser spot on sample was 300 μm obtained after calibration and focusing of the laser.

6.4. Electron microscopy

Micrographs of the surface and radial distribution of chemical elements were collected by high-resolution field-emission electron microscope *Zeiss Ultra-55 plus* equipped with energy-dispersive X-ray (EDX) analysis unit.

6.5. Heat transfer simulations

The modeling was performed in COMSOL Multiphysics 5.2 simulation package. We used non-stationary thermal conductivity equation for heat transfer calculations:

$$C_p \frac{\partial T}{\partial t} - \lambda \Delta T + L \frac{\partial g}{\partial t} = \alpha A I_0 e^{\left(\frac{x^2+y^2}{r^2}\right)-\alpha z} \phi(t)$$

where C_p is heat capacity, λ - thermal conductivity, L - enthalpy of fusion, g - proportion of hard phases, α - absorption coefficient, T - flow temperature, A - emissivity, x and y – coordinates on the surface of the sample such that the origin corresponds to the center of the laser spot, $\phi(t)$ - temporal profile of the laser beam intensity and τ - duration of the pulse. The heat source emulating laser pulse followed Beer–Lambert–Bouguer law. The model takes into account

Symbol	Name	Value	Reference
λ	Thermal conductivity	5.3 W/(m·K)	[51]
ρ	Density	7177 kg/m^3	[51]
C_p	Heat capacity	$C_p(T)$ J/(kg·K)	[51]
L	Enthalpy of fusion	91 J/g	[51]
A	Emissivity	0.13 1/T	[52]
T_g	Glass transition temperature	715 K	This work (DSC)
T_c	Crystallization temperature	757 K	This work (DSC)
T_S	Solidus temperature	1091 K	[51]
T_L	Liquidus temperature	1228 K	[51]
$T_{S\to L}$	Solidus-liquidus range	137 K	[51]

Table 1: Parameters of the sample.

temperature dependence of the heat capacity. Latent heat of fusion was also included into calculations.

The sample was assumed to be infinite because of the small size of the heat-affected area compared to the sample dimensions. Gaussian distribution was assumed for the profile of energy in the laser spot. Parameters of the simulation are summarized in Table 1.

References

[1] C. Suryanarayana, A. Inoue, Bulk Metallic Glasses, CRC Press, 2010.

[2] W. Wang, C. Dong, C. Shek, Bulk metallic glasses, Materials Science and Engineering: R: Reports 44 (2) (2004) 45 – 89. doi:https://doi.org/10.1016/j.mser.2004.03.001. URL http://www.sciencedirect.com/science/article/pii/S0927796X04000300

[3] A. Inoue, Stabilization of metallic supercooled liquid and bulk amorphous alloys, Acta Materialia 48 (1) (2000) 279 – 306. doi:https://doi.org/10.1016/S1359-6454(99)00300-6. URL http://www.sciencedirect.com/science/article/pii/S1359645499003006

[4] A. R. Yavari, J. J. Lewandowski, J. Eckert, Mechanical properties of bulk metallic glasses, MRS Bulletin 32 (8) (2007) 635–638. doi:10.1557/mrs2007.125.

[5] A. L. Greer, Metallic glasses on the threshold, Materials Today 12 (1) (2009) 14 – 22. doi:https://doi.org/10.1016/S1369-7021(09)70037-9. URL http://www.sciencedirect.com/science/article/pii/S1369702109700379

[6] B. Chen, T. Shi, M. Li, F. Yang, F. Yan, G. Liao, Laser welding of annealed $Zr_{55}Cu_{30}Ni_5Al_{10}$ bulk metallic glass, Intermetallics 46 (Supplement C) (2014) 111 – 117. doi:https://doi.org/10.1016/j.intermet.2013.11.008.
URL http://www.sciencedirect.com/science/article/pii/S0966979513003075

[7] H.-S. Wang, M.-S. Chiou, H.-G. Chen, J. S.-C. Jang, The effects of initial welding temperature and welding parameters on the crystallization behaviors of laser spot welded Zr-based bulk metallic glass, Materials Chemistry and Physics 129 (1) (2011) 547 – 552. doi:https://doi.org/10.1016/j.matchemphys.2011.04.067.
URL http://www.sciencedirect.com/science/article/pii/S0254058411003798

[8] H.-S. Wang, Y.-Z. Su, J. S.-C. Jang, H.-G. Chen, A comparison of crystallization behaviors of laser spot welded Zr-Cu-Ag-Al and Zr-Cu-Ni-Al bulk metallic glasses, Materials Chemistry and Physics 139 (1) (2013) 215 – 219. doi:https://doi.org/10.1016/j.matchemphys.2013.01.025.
URL http://www.sciencedirect.com/science/article/pii/S0254058413000692

[9] J. Qiao, J. Pelletier, Dynamic mechanical relaxation in bulk metallic glasses: A review, Journal of Materials Science & Technology 30 (6) (2014) 523 – 545. doi:https://doi.org/10.1016/j.jmst.2014.04.018.
URL http://www.sciencedirect.com/science/article/pii/S1005030214000930

[10] J. J. L. *, W. H. Wang, A. L. Greer, Intrinsic plasticity or brittleness of metallic glasses, Philosophical Magazine Letters 85 (2) (2005) 77–87. arXiv:http://dx.doi.org/10.1080/09500830500080474, doi:10.1080/09500830500080474.
URL http://dx.doi.org/10.1080/09500830500080474

[11] Z. Zhu, V. Dhokia, A. Nassehi, S. Newman, A review of hybrid manufacturing processes – state of the art and future perspectives, International Journal of Computer Integrated Manufacturing 26 (7) (2013) 596–615. arXiv:https://doi.org/10.1080/0951192X.2012.749530, doi:10.1080/0951192X.2012.749530.
URL https://doi.org/10.1080/0951192X.2012.749530

[12] B. Chen, T. Shi, M. Li, Z. Zhang, Z. Zhu, G. Liao, Laser welding of $Zr_{41}Ti_{14}Cu_12Ni_{10}Be_{23}$ bulk metallic glass: Experiment and temperature field simulation, Advanced Engineering Materials 15 (5) (2013) 407–413. doi:10.1002/adem.201200308.
URL http://dx.doi.org/10.1002/adem.201200308

[13] E. Williams, E. Brousseau, Nanosecond laser processing of $Zr_{41.2}Ti_{13.8}Cu_{12.5}Ni_{10}Be_{22.5}$ with single pulses, Journal of Materials Processing Technology 232 (Supplement C) (2016) 34 – 42. doi:https://doi.org/10.1016/j.jmatprotec.2016.01.023. URL http://www.sciencedirect.com/science/article/pii/S0924013616300231

[14] N. Tariq, B. Hasan, J. Akhter, Evolution of microstructure in $Zr_{55}Cu_{30}Al_{10}Ni_5$ bulk amorphous alloy by high power pulsed Nd:YAG laser, Journal of Alloys and Compounds 485 (1) (2009) 212 – 214. doi:https://doi.org/10.1016/j.jallcom.2009.06.008. URL http://www.sciencedirect.com/science/article/pii/S0925838809011505

[15] G. Yang, X. Lin, F. Liu, Q. Hu, L. Ma, J. Li, W. Huang, Laser solid forming Zr-based bulk metallic glass, Intermetallics 22 (Supplement C) (2012) 110 – 115. doi:https://doi.org/10.1016/j.intermet.2011.10.008. URL http://www.sciencedirect.com/science/article/pii/S0966979511003220

[16] J. Fu, Y. Zhu, C. Zheng, R. Liu, Z. Ji, Evaluate the effect of laser shock peening on plasticity of Zr-based bulk metallic glass, Optics & Laser Technology 73 (Supplement C) (2015) 94 – 100. doi:https://doi.org/10.1016/j.optlastec.2015.04.009. URL http://www.sciencedirect.com/science/article/pii/S0030399215001036

[17] Y. Zhu, J. Fu, C. Zheng, Z. Ji, Effect of laser shock peening without absorbent coating on the mechanical properties of Zr-based bulk metallic glass, Optics & Laser Technology 75 (Supplement C) (2015) 157 – 163. doi:https://doi.org/10.1016/j.optlastec.2015.06.029. URL http://www.sciencedirect.com/science/article/pii/S0030399215001917

[18] H.-K. Lin, C.-J. Lee, T.-T. Hu, C.-H. Li, J. Huang, Pulsed laser micromachining of Mg-Cu-Gd bulk metallic glass, Optics and Lasers in Engineering 50 (6) (2012) 883 – 886. doi:https://doi.org/10.1016/j.optlaseng.2012.01.003. URL http://www.sciencedirect.com/science/article/pii/S0143816612000048

[19] E. Williams, N. Lavery, Laser processing of bulk metallic glass: A review, Journal of Materials Processing Technology 247 (Supplement C) (2017) 73 – 91. doi:https://doi.org/10.1016/j.jmatprotec.2017.03.034. URL http://www.sciencedirect.com/science/article/pii/S0924013617301279

[20] J. J. Lewandowski, A. L. Greer, Temperature rise at shear bands in metallic glasses, Nature Materials 5 (1) (2006) 15 – 18.
URL http://dx.doi.org/10.1038/nmat1536

[21] T. B. Britton, F. P. E. Dunne, A. J. Wilkinson, On the mechanistic basis of deformation at the microscale in hexagonal close-packed metals, Proceedings of the Royal Society of London A: Mathematical, Physical and Engineering Sciences 471 (2178). arXiv:http://rspa.royalsocietypublishing.org/content/471/2178/20140881.full.pdf, doi:10.1098/rspa.2014.0881.
URL http://rspa.royalsocietypublishing.org/content/471/2178/20140881

[22] C. A. Volkert, A. Donohue, F. Spaepen, Effect of sample size on deformation in amorphous metals, Journal of Applied Physics 103 (8) (2008) 083539. doi:10.1063/1.2884584.
URL http://dx.doi.org/10.1063/1.2884584

[23] G. Kumar, A. Desai, J. Schroers, Bulk metallic glass: the smaller the better, Advanced materials 23 (4) (2011) 461–76.
URL https://doi.org/10.1002/adma.201002148

[24] M. Gao, J. Dong, Y. Huan, Wang, Y. Tian, W.-H. Wang, Macroscopic tensile plasticity by scalarizating stress distribution in bulk metallic glass, Advanced materials 6 (2016) 21929.
URL http://dx.doi.org/10.1038/srep21929

[25] K. K. Song, S. Pauly, B. A. Sun, J. Tan, M. Stoica, U. Kühn, J. Eckert, Correlation between the microstructures and the deformation mechanisms of CuZr-based bulk metallic glass composites, AIP Advances 3 (1) (2013) 012116. doi:10.1063/1.4789516.

[26] M. Zhang, D. Yao, Z. Cao, P. Li, P. Zhou, X. Wang, Influence of oxidation on the performance of $Zr_{55}Cu_{30}Al_{10}Ni_5$ bmg, Intermetallics 79 (Supplement C) (2016) 20 – 27. doi:https://doi.org/10.1016/j.intermet.2016.08.007.
URL http://www.sciencedirect.com/science/article/pii/S0966979516300486

[27] G. Wu, R. Li, Z. Liu, B. Chen, Y. Li, Y. Cai, T. Zhang, Induced multiple heterogeneities and related plastic improvement by laser surface treatment in CuZr-based bulk metallic glass, Intermetallics 24 (2012) 50 – 55. doi:https://doi.org/10.1016/j.intermet.2012.01.022.
URL http://www.sciencedirect.com/science/article/pii/S0966979512000441

[28] Laser micromachining of metallic glasses: investigation of the material response to machining with micro-second and pico-second lasers, Vol. 7584.

[29] S. Zinkle, G. Was, Materials challenges in nuclear energy, Acta Materialia 61 (3) (2013) 735 – 758, the Diamond Jubilee Issue. doi:https://doi.org/10.1016/j.actamat.2012.11.004.
URL http://www.sciencedirect.com/science/article/pii/S1359645412007987

[30] J. H. Cavka, S. Jakobsen, U. Olsbye, N. Guillou, C. Lamberti, S. Bordiga, K. P. Lillerud, A new zirconium inorganic building brick forming metal organic frameworks with exceptional stability, Journal of the American Chemical Society 130 (42) (2008) 13850–13851, pMID: 18817383. arXiv:https://doi.org/10.1021/ja8057953, doi:10.1021/ja8057953.
URL https://doi.org/10.1021/ja8057953

[31] L. L. Hench, J. Wilson, An Introduction to Bioceramics, WORLD SCIENTIFIC, 1993. arXiv:https://www.worldscientific.com/doi/pdf/10.1142/2028, doi:10.1142/2028.
URL https://www.worldscientific.com/doi/abs/10.1142/2028

[32] S. B. Chaabene, L. Bergaoui, A. Ghorbel, J.-F. Lambert, Non-aggressive way using zirconium acetate for preparation of zirconium pillared clay developing high sulfur thermal stability over 830 ^{o}c, in: E. Gaigneaux, D. D. Vos, P. Grange, P. Jacobs, J. Martens, P. Ruiz, G. Poncelet (Eds.), Scientific Bases for the Preparation of Heterogeneous Catalysts, Vol. 143 of Studies in Surface Science and Catalysis, Elsevier, 2000, pp. 1053 – 1062. doi:https://doi.org/10.1016/S0167-2991(00)80751-X.
URL http://www.sciencedirect.com/science/article/pii/S016729910080751X

[33] M. Marcellini, F. M. Fernandes, D. Dedovets, S. Deville, Water/ice phase transition: The role of zirconium acetate, a compound with ice-shaping properties, The Journal of Chemical Physics 146 (14) (2017) 144504. arXiv:https://doi.org/10.1063/1.4979845, doi:10.1063/1.4979845.
URL https://doi.org/10.1063/1.4979845

[34] Q. Chen, L. Liu, S.-M. Zhang, The potential of zr-based bulk metallic glasses as biomaterials, Frontiers of Materials Science in China 4 (1) (2010) 34–44. doi:10.1007/s11706-010-0004-5.
URL https://doi.org/10.1007/s11706-010-0004-5

[35] B. Ganem, R. R. Franke, Paclitaxel from primary taxanes: A perspective on creative invention in organozirconium chemistry, The Journal of Organic Chemistry 72 (11) (2007) 3981–3987. arXiv:https://doi.org/10.1021/jo070129s, doi:10.1021/jo070129s.
URL https://doi.org/10.1021/jo070129s

[36] D. Duraccio, F. Mussano, M. G. Faga, Biomaterials for dental implants: current and future trends, Journal of Materials Science 50 (14) (2015) 4779–4812. doi:10.1007/s10853-015-9056-3.
URL https://doi.org/10.1007/s10853-015-9056-3

[37] W. H. Cao, J. L. Zhang, C. H. Shek, The oxidation behavior of $Cu_{42}Zr_{42}Al_8Ag_8$ bulk metallic glasses, Journal of Materials Science 48 (3) (2013) 1141–1146. doi:10.1007/s10853-012-6851-y.
URL https://doi.org/10.1007/s10853-012-6851-y

[38] W. Kai, I. Ren, B. Barnard, P. Liaw, M. Demetriou, W. Johnson, Oxidation behavior of a pd43cu27ni10p20 bulk metallic glass and foam in dry air, Metallurgical and Materials Transactions A 41 (7) (2010) 1720–1725. doi:10.1007/s11661-010-0231-5.
URL https://doi.org/10.1007/s11661-010-0231-5

[39] S. V.Yu, Influence of hydrogen and oxygen sorption and desorption on processes of modification and crystallization of alloys, Casting and metallurgy 3 (56) (2010) 91 – 96, (In Russian).

[40] G. V. M. Chernyaeva T.P., Stukalov A.I., Behavior of oxygen in zirconium, in: Oxygen in zirconium, Ukraine, 1999, (Original title: Kislorod v tcirkonii).

[41] K. B. Kuznetsov, I. A. Kovalev, V. Y. Zufman, A. I. Ogarkov, S. V. Shevtsov, A. A. Ashmarin, A. S. Chernyavskii, K. A. Solntsev, Kinetics of zirconium saturation with nitrogen during high-temperature nitridation, Inorganic Materials 52 (6) (2016) 558–560. doi:10.1134/S0020168516060078.
URL https://doi.org/10.1134/S0020168516060078

[42] L. Krusin-Elbaum, M. Wittmer, Oxidation kinetics of zrn thin films, Thin Solid Films 107 (1) (1983) 111 – 116. doi:https://doi.org/10.1016/0040-6090(83)90013-5.
URL http://www.sciencedirect.com/science/article/pii/0040609083900135

[43] J. Belle, M. W. Mallett, Kinetics of the high temperature oxidation of zirconium, Journal of The Electrochemical Society 101 (7) (1954) 339–342. arXiv:http://jes.ecsdl.org/content/101/7/339.full.pdf+html, doi:10.1149/1.2781278.
URL http://jes.ecsdl.org/content/101/7/339.abstract

[44] Y. Zhu, K. Mimura, M. Isshiki, Oxidation mechanism of copper at 623-1073 k, MATERIALS TRANSACTIONS 43 (9) (2002) 2173–2176. doi:10.2320/matertrans.43.2173.

[45] W. W. Smeltzer, Oxidation of aluminum in the temperature range 400^o-600 ^{o}c, Journal of The Electrochemical Society 103 (4) (1956) 209–214. arXiv:http://jes.ecsdl.org/content/103/4/209.full.pdf+html, doi:10.1149/1.2430279.
URL http://jes.ecsdl.org/content/103/4/209.abstract

[46] H. Huang, N. Jun, M. Jiang, M. Ryoko, J. Yan, Nanosecond pulsed laser irradiation induced hierarchical micro/nanostructures on zr-based metallic glass substrate, Materials and Design 109 (2016) 153–161. doi:10.1016/j.matdes.2016.07.056.

[47] W. J. Boettinger, D. Shechtman, R. J. Schaefer, F. S. Biancaniello, The effect of rapid solidification velocity on the microstructure of Ag-Cu alloys, Metallurgical Transactions A 15 (1) (1984) 55–66. doi:10.1007/BF02644387.
URL https://doi.org/10.1007/BF02644387

[48] Q. Pan, W. Huang, X. Lin, Y. Zhou, Primary spacing selection of CuMn alloy under laser rapid solidification condition, Journal of Crystal Growth 181 (1) (1997) 109 – 116. doi:https://doi.org/10.1016/S0022-0248(97)00273-X.
URL http://www.sciencedirect.com/science/article/pii/S002202489700273X

[49] D. J. F. W. Kurz, Fundamentals of Solidification, CRC Press, 1992.

[50] W. Kurz, B. Giovanola, R. Trivedi, Theory of microstructural development during rapid solidification, Acta Metallurgica 34 (5) (1986) 823 – 830. doi:https://doi.org/10.1016/0001-6160(86)90056-8.
URL http://www.sciencedirect.com/science/article/pii/0001616086900568

[51] Q. Jiang, X. Wang, X. Nie, G. Zhang, H. Ma, H.-J. Fecht, J. Bendnarcik, H. Franz, Y. Liu, Q. Cao, J. Jiang, Zr-(Cu,Ag)-Al bulk metallic glasses, Acta Materialia 56 (8) (2008) 1785 – 1796. doi:https://doi.org/10.1016/j.actamat.2007.12.030.
URL http://www.sciencedirect.com/science/article/pii/S1359645407008609

[52] S. Atallah, A relationship between emissivity and thermal conductivity of metals, British Journal of Applied Physics 17 (4) (1966) 573.
URL http://stacks.iop.org/0508-3443/17/i=4/a=120